# Higgs boson decays to $\gamma$ and invisible particles in the standard model

Yi Sun* and Dao-Neng Gao†

*Interdisciplinary Center for Theoretical Study, University of Science and Technology of China, Hefei, Anhui 230026, China*

(Received 5 November 2013; published 28 January 2014)

Using the Higgs boson mass $m_h = 125$ GeV, the radiative Higgs decays $h \to \gamma\nu_l\bar{\nu}_l$ with $\nu_l = \nu_e, \nu_\mu$, and $\nu_\tau$ are analyzed in the standard model. Our calculation shows that the inclusive width of these processes, i.e., the sum of $\Gamma(h \to \gamma\nu_l\bar{\nu}_l)$ for $\nu_l = \nu_e, \nu_\mu, \nu_\tau$, is 1.41 keV, which is about 15% of $\Gamma(h \to \gamma\gamma)$. Therefore, the observation of these channels in future precise experiments may provide some useful information on the Higgs physics in both the standard model and its possible extensions.

DOI: 10.1103/PhysRevD.89.017301 PACS numbers: 14.80.Bn, 12.38.Bx

The discovery of the Higgs-like particle at around 125 GeV—thanks to the hard work of the ATLAS [1] and CMS [2] Collaborations at the Large Hadron Collider—is a big triumph of the high energy physics community. Since elementary particles in the standard model (SM) become massive via the Higgs mechanism [3], the Higgs sector plays a key role in our understanding of the nature of the world. Thus it is very important to identify the new resonance with the elementary Higgs boson in the SM. ATLAS [1] and CMS [2] have observed several decay channels of this Higgs-like particle, including the $\gamma\gamma$, $ZZ^*$, $WW^*$, $bb$, and $\tau\tau$ channels, and have found that its properties are consistent with the SM Higgs boson.

Due to the increasing amount of experimental data, in addition to the above dominant decay channels some rare decay modes will also be interesting. The radiative decays $h \to \gamma l^+ l^-$ have been analyzed both theoretically [4–13] and experimentally [14,15]. In the present paper, we will study another rare decay channel, $h \to \gamma\nu_l\bar{\nu}_l$, with $\nu_l = \nu_e$, $\nu_\mu$, and $\nu_\tau$. Obviously, only a photon—or, more accurately, a photon and missing energy [16]—can be experimentally observed in these decays. On the other hand, in the new physics, the decay channel $h \to \gamma + \text{invisible}$ is more complex than that in the SM, where the invisible particles could be (besides neutrinos) other new particles that are absent in the SM. Model independently, in Ref. [17] the Higgs decay mode involving a photon together with one or two invisible particles was investigated using effective interactions. Some specific models have been studied: the mode $h \to \gamma Z_d$, where $Z_d$ is a light vector boson associated to a "dark sector" U(1) gauge group, was analyzed in Ref. [18]; in the next-to-minimal supersymmetric standard model, the process $h \to \gamma\chi_1\chi_1$, where $\chi_1$ is the lightest supersymmetry particle and is invisible in the experiments, may be interesting in some parameter space [19]; the Higgs decay to a photon and two gravitinos was studied in Ref. [20], which can be important in scenarios where the supersymmetry-breaking scale is of the order of a few TeV. Therefore, in order to analyze these exotic decays in the new physics beyond the SM, we should first evaluate their contributions in the SM. Only after we fully understand their SM background can the future precise experimental study of the $h \to \gamma\nu_l\bar{\nu}_l$ decays possibly provide us with some useful information on the Higgs sector in new physics scenarios.

In the SM, the tree-level contribution of the processes $h \to \gamma\nu_l\bar{\nu}_l$ is forbidden and the lowest-order contribution is given by the one-loop diagrams. The typical one-loop Feynman diagrams for these processes are shown in Figs. 1 and 2, respectively, which are of two basic types: (i) the $Z^*$-pole three-point diagrams via $h \to \gamma Z^* \to \gamma\nu_l\bar{\nu}_l$ (Fig. 1), and (ii) the four-point box diagrams involving the $W$ gauge boson and the charged lepton $l$ inside the loop (Fig. 2), where the photon is emitted from the $W$ or $l$ internal lines.

The amplitude of $h \to \gamma\nu_l\bar{\nu}_l$ at the one-loop level can be expressed as

$$\mathcal{M} = \mathcal{M}_{\text{tri}} + \mathcal{M}_{\text{box}}, \tag{1}$$

where $\mathcal{M}_{\text{tri}}$ and $\mathcal{M}_{\text{box}}$ denote the amplitudes of the three-point and four-point diagrams, respectively,

$$\mathcal{M}_{\text{tri}} = \varepsilon^{\nu*}(p) C_1 (p_\mu q_\nu - g_{\mu\nu} p\cdot q)\bar{u}(k_2)\gamma^\mu P_L v(k_1), \tag{2}$$

$$\mathcal{M}_{\text{box}} = \varepsilon^{\nu*}(p)\bar{u}(k_2)[(C_2 k_1^\nu + C_3 k_2^\nu)\not{p} P_L - (C_2 k_1\cdot p + C_3 k_2\cdot p)\gamma^\nu P_L] v(k_1), \tag{3}$$

with $P_L = (1-\gamma^5)/2$. One can check that the amplitudes of the three-point and four-point diagrams are separately gauge invariant. The expressions for the $C_i$'s in the amplitudes are

$$C_1 = P_Z \frac{\alpha_e^2}{\sqrt{2} m_W \sin^3\theta_W}\left[-\frac{\cos\theta_W}{2m_W^2} I_1 - \frac{2N_c^f Q_f m_f^2}{(m_h^2 - q^2)^2 \cos\theta_W} \times (T_f - 2Q_f \sin^2\theta_W) I_2\right], \tag{4}$$

*sunyi@mail.ustc.edu.cn
†gaodn@ustc.edu.cn

 

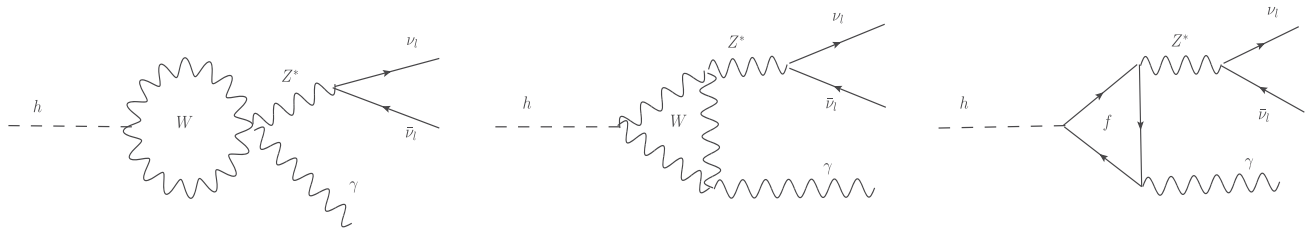


FIG. 1. Three-point diagrams for $h \to \gamma\nu_l\bar{\nu}_l$.

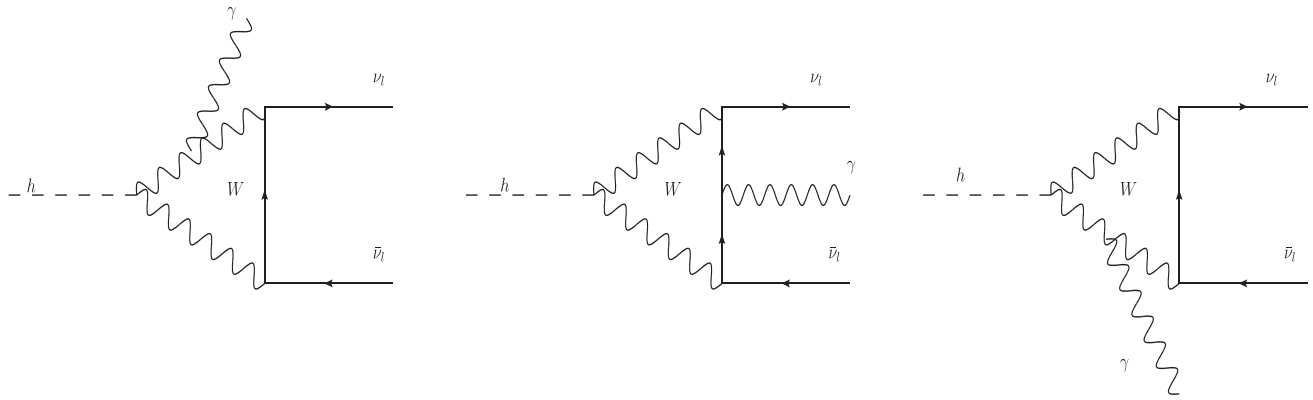


FIG. 2. Four-point diagrams for $h \to \gamma\nu_l\bar{\nu}_l$.

$$C_2 = \frac{-\alpha_e^2}{2m_W \sin^3\theta_W} I_3, \tag{5}$$

$$C_3 = \frac{-\alpha_e^2}{2m_W \sin^3\theta_W} I_4. \tag{6}$$

Here $\alpha_e$ is the fine-structure constant and $\theta_W$ is the electroweak mixing angle. $m_f$ is the mass, $N_c^f$ is the color multiplicity, $Q_f$ (in units of $e$) is the charge, and $T_f$ is the third component of weak isospin of the fermion $f$ inside the fermion loop in Fig. 1. $k_1$, $k_2$, and $p$ represent the momentum of $\nu_l$, $\bar{\nu}_l$, and $\gamma$ in the final states, respectively. We denote $q$ as the momentum of the virtual particle $Z^*$ in Fig. 1, $q^2 = (k_1 + k_2)^2$ is the neutrino pair mass squared, and $P_Z$ is from the propagator of the virtual $Z^*$ gauge boson, which reads

$$P_Z = \frac{1}{q^2 - m_Z^2 + i m_Z \Gamma_Z}. \tag{7}$$

The notations for the $I_i$'s are given by

$$I_1 = -8m_W^2(4m_W^2 - q^2)C_0^0 - 4(12m_W^4 + 4m_W^2 q^2 - q^2 m_h^2)(C_1^0 + C_{11}^0 + C_{12}^0), \tag{8}$$

$$I_2 = -2q^2 B_0(m_h^2, m_f^2, m_f^2) + 2q^2 B_0(q^2, m_f^2, m_f^2) + (m_h^2 - q^2)(-2 + (m_h^2 - q^2 - 4m_f^2)C_0(0, q^2, m_h^2, m_f^2, m_f^2, m_f^2)), \tag{9}$$

$$\begin{aligned} I_3 = {} & -4C_0^4 + 2C_1^2 - 2C_2^2 + 4(1 + a + b + f)C_{12}^4 + l^2(C_2^3 - C_{12}^1 + C_{12}^3 + C_{22}^3) \\ & + 2m_W^2[3D_1^2 + 2D_2^2 - D_3^2 + D_1^3 + D_3^3 - l^2(D_0^1 + D_0^2 + D_0^3) - (-2 + l^2(b + f))D_2^1 \\ & - (2 + l^2 + a l^2)D_3^1 + (2 + l^2(1 + a + b + f)(D_{23}^3 - D_{23}^1 - D_{23}^2 - D_{33}^1 - D_{33}^2 - D_2^2))], \end{aligned} \tag{10}$$

$$\begin{aligned} I_4 = {} & -2(C_0^2 + C_1^2 + 2C_2^2 + 2C_0^4) + 4(1 + a + b + f)C_{12}^4 + l^2(C_1^5 + C_{12}^5 + C_{22}^5 + C_2^6 + C_{12}^6 + C_{22}^6) \\ & - 2m_W^2[l^2(D_0^1 + D_0^2 + D_0^3) + 2(D_1^1 + D_1^2 + D_1^3 + D_2^3) + (2 + l^2(1 + a + b + f)) \\ & \times (D_{12}^1 + D_{13}^1 + D_{13}^2 - D_2^3 - D_{12}^3 - D_{22}^3)], \end{aligned} \tag{11}$$

with the following dimensionless parameters: $a = k_1 \cdot p/m_W^2$, $b = k_2 \cdot p/m_W^2$, $f = k_1 \cdot k_2/m_W^2$, and $l = m_l/m_W$, where $m_l$ is the mass of the charged lepton in the four-point diagrams.[1] The notations for the $C_i^j$'s and $D_i^j$'s read

$$
\begin{aligned}
C_i^0 &= C_i(0, q^2, m_h^2, m_W^2, m_W^2, m_W^2),\\
C_i^1 &= C_i(0, 2k_1 \cdot p, 0, m_l^2, m_l^2, m_W^2),\\
C_i^2 &= C_i(0, m_h^2, 2k_2 \cdot p, m_l^2, m_W^2, m_W^2),\\
C_i^3 &= C_i(0, 0, 2k_1 \cdot p, m_w^2, m_W^2, m_l^2),\\
C_i^4 &= C_i(0, m_h^2, 2k_1 \cdot k_2, 0, m_W^2, m_W^2, m_W^2),\\
C_i^5 &= C_i(2k_2 \cdot p, 0, 0, m_l^2, m_W^2, m_W^2),\\
C_i^6 &= C_i(0, 0, 2k_2 \cdot p, m_W^2, m_l^2, m_l^2),\\
D_i^1 &= D_i(0, 2k_2 \cdot p, 0, 2k_1 \cdot p, 0, m_h^2, m_l^2, m_W^2, m_l^2, m_W^2),\\
D_i^2 &= D_i(0, 2k_1 \cdot k_2, 0, 2k_1 \cdot p, 0, m_h^2, m_l^2, m_W^2, m_W^2, m_W^2),\\
D_i^3 &= D_i(0, 0, m_h^2, 0, 2k_2 \cdot p, 2k_1 \cdot k_2, m_l^2, m_W^2, m_W^2, m_W^2),
\end{aligned}
\tag{12}
$$

where the $C_i$'s and $D_i$'s are the three-point and four-point Feynman integrals defined in Ref. [21], respectively.

The differential decay rate of $h \to \gamma\nu_l\bar{\nu}_l$, including both three-point and four-point diagram contributions, can be expressed as

$$
\begin{aligned}
\frac{d\Gamma}{dE_\gamma d\cos\theta} = \frac{m_h^2 E_\gamma^3 (m_h - 2E_\gamma)}{128\pi^3} &[|C_1|^2(1+\cos^2\theta)\\
&+ 2|C_2|^2 \sin^4(\theta/2) + 2|C_3|^2\cos^4(\theta/2)\\
&+ 4\,\mathrm{Re}[C_1 C_2^*]\sin^4(\theta/2)\\
&+ 4\,\mathrm{Re}[C_1 C_3^*]\cos^4(\theta/2)],
\end{aligned}
\tag{13}
$$

where $E_\gamma$ is the photon energy in the rest frame of the Higgs boson, and in this frame we have $q^2 = m_h^2 - 2m_h E_\gamma$. $\theta$ is the angle between the three-momentum of the Higgs boson and the three-momentum of $\nu$ in the rest frame of the neutrino pair (since the neutrino cannot be observed experimentally, $\theta$ should be integrated out later). The range of these two variables is given by

$$
0 \le E_\gamma \le \frac{m_h}{2}, \qquad -1 \le \cos\theta \le 1. \tag{14}
$$

The first term in Eq. (13) is from the three-point diagrams and will dominate the differential decay rate, the second and third terms are induced from the four-point diagrams, and the last two terms are contributed by the interference between the three-point and four-point diagrams.

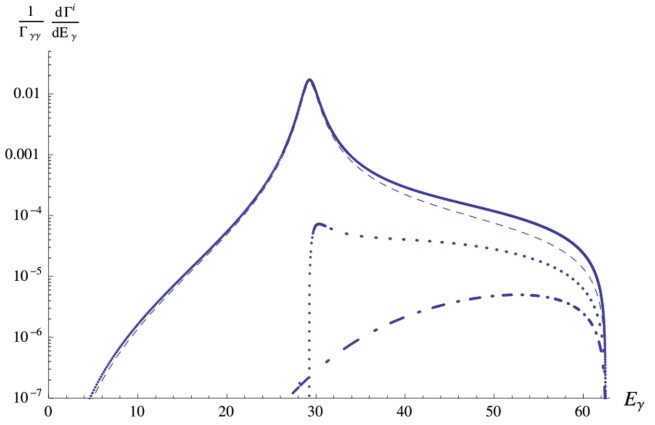


FIG. 3 (color online). The decay spectrum for $h \to \gamma\nu_e\bar{\nu}_e$ normalized by $\Gamma(h \to \gamma\gamma)$ (denoted as $\Gamma_{\gamma\gamma}$). The dashed line denotes the contribution of the three-point diagrams, the dotted line shows the behavior of the interference between the three-point and four-point diagrams, and the dot-dashed line shows the contribution from the four-point diagrams. The solid line gives the total contributions.

After integrating over $\cos\theta$ in Eq. (13), one can get the decay spectrum $d\Gamma/dE_\gamma$. The $h \to \gamma\nu_e\bar{\nu}_e$ decay spectrum, normalized by $\Gamma(h \to \gamma\gamma)$, is displayed in Fig. 3. Different types of contributions—including the three-point and four-point diagrams, and their interference—are plotted separately for comparison. From these plots, one can find that the differential cross section of the three-point diagrams are enhanced when $E_\gamma \sim 30$ GeV. The reason for this is that $\sqrt{q^2}$ is close to $m_Z$ and the virtual gauge boson $Z^*$ is almost on-shell at this time. Also, one can easily find that the three-point diagrams give the dominant contribution, while the contribution from the four-point diagrams is very small. It is easy to see that the amplitude (2) and differential decay rate in Eq. (13) from the dominant three-point diagrams—if the small mass of the neutrinos is neglected—have no difference for different types of neutrinos in the final states. Therefore it is expected that the decay spectrum for the $\nu_\mu$ and $\nu_\tau$ modes will be very similar to the case of the $\nu_e$ mode, as is already shown in Fig. 3. Actually, we have confirmed this point in our numerical analysis.

The decay rate of $h \to \gamma\nu_l\bar{\nu}_l$ can be obtained by integrating $E_\gamma$ in the decay spectrum $d\Gamma/dE_\gamma$, so we get

$$
\Gamma(h \to \gamma\nu_e\bar{\nu}_e) = 0.47\ \mathrm{keV}, \tag{15}
$$

in which the contribution of the three-point diagrams is $\Gamma(h \to \gamma Z^* \to \gamma\nu_e\bar{\nu}_e) = 0.447$ keV. Since the four-point diagrams give very small contributions, both the charged lepton and neutrino masses can actually be neglected in our numerical calculations. This will lead to the same results as Eq. (15) for the $\nu_\mu$ and $\nu_\tau$ modes. Experimentally, the neutrinos are invisible—only a single photon and missing

[1]One should take care of the difference between $m_f$, which is the mass of the fermion inside the fermion loop of the three-point diagrams, and $m_l$, which is the mass of the charged lepton in the four-point diagrams.

energy can be observed—so the decay rate of the Higgs to a photon and invisible particles in the SM is

$$\Gamma(h \to \gamma + \text{invisible}) = \sum_{\nu_l=\nu_e,\nu_\mu,\nu_\tau} \Gamma(h \to \gamma\nu_l\bar{\nu}_l) = 1.41\ \text{keV} = 15.2\%\Gamma(h \to \gamma\gamma). \quad (16)$$

In conclusion, we have analyzed the rare decay modes $h \to \gamma\nu_l\bar{\nu}_l$ with $\nu_l = \nu_e$, $\nu_\mu$, and $\nu_\tau$ in the SM. It was found that these processes are dominated by the $Z^*$-pole transition $h \to \gamma Z^* \to \gamma\nu_l\bar{\nu}_l$, and that four-point box diagrams only give very small contributions. The theoretical prediction of the decay rate in the SM is quite under control, as shown in Eqs. (15) and (16). Therefore, in future high-statistics experiments such as a Higgs factory the investigation of the $h \to \gamma +$ invisible decays could be very interesting both to increase our understanding of the properties of the SM Higgs boson and to explore the novel Higgs dynamics in new physics scenarios.

This work was supported in part by the NSF of China under Grant Nos. 11075149 and 11235010.

[1] ATLAS Collaboration, Phys. Lett. B **716**, 1 (2012).
[2] CMS Collaboration, Phys. Lett. B **716**, 30 (2012); CMS Collaboration, J. High Energy Phys. 06 (**2013**) 081.
[3] F. Englert and E. Brout, Phys. Rev. Lett. **13**, 321 (1964); P. W. Higgs, Phys. Lett. **12**, 132 (1964); Phys. Rev. Lett. **13**, 508 (1964); Phys. Rev. **145**, 1156 (1966); G. S. Guramik, C. R. Hagen, and T. W. B. Kibble, Phys. Rev. Lett. **13**, 585 (1964); T. W. B. Kibble, Phys. Rev. **155**, 1554 (1967).
[4] A. Abbasabadi, D. Bowser-Chao, D. A. Dicus, and W. W. Repko, Phys. Rev. D **55**, 5647 (1997).
[5] C. S. Li, S. H. Zhu, and C. F. Qiao, Phys. Rev. D **57**, 6928 (1998).
[6] A. Abbasabadi and W. W. Repko, Phys. Rev. D **62**, 054025 (2000).
[7] A. Firan and R. Stroynowski, Phys. Rev. D **76**, 057301 (2007).
[8] L. B. Chen, C. F. Qiao, and R. L. Zhu, Phys. Lett. B **726**, 306 (2013).
[9] D. A. Dicus and W. W. Repko, Phys. Rev. D **87**, 077301 (2013).
[10] A. Y. Korchin and V. A. Kovalchuk, Phys. Rev. D **88**, 036009 (2013).
[11] Y. Sun, H.-R. Chang, and D.-N. Gao, J. High Energy Phys. 05 (**2013**) 061.
[12] G. Passarino, Phys. Lett. B **727**, 424 (2013).
[13] D. A. Dicus, C. Kao, and W. W. Repko, arXiv:1310.4380.
[14] ATLAS Collaboration, Report No. ATLAS-CONF-2013-009.
[15] CMS Collaboration, Phys. Lett. B **726**, 587 (2013).
[16] ATLAS Collaboration, Eur. Phys. J. C **72**, 1844 (2012).
[17] J. F. Kamenik and C. Smith, Phys. Rev. D **85**, 093017 (2012).
[18] H. Davoudiasl, H.-S. Lee, I. Lewis, and W. J. Marciano, Phys. Rev. D **88**, 015022 (2013).
[19] D. Curtin *et al.*, arXiv:1312.4992; T. Liu, Exotic Decays of the 125 GeV Higgs, talk at the University of Science and Technology of China, September, 2013.
[20] C. Petersson, A. Romagnoni, and R. Torre, J. High Energy Phys. 10 (**2012**) 016.
[21] G. Passarino and M. Veltman, Nucl. Phys. **B160**, 151 (1979); R. Mertig, Guide to FeynCalc 1.0 (1992), available at http://physics.indiana.edu/~sg/p622/FCGuide3.ps; T. Hahn and M. Perez-Victoria, Comput. Phys. Commun. **118**, 153 (1999); Y. Sun and H.-R. Chang, Chin. Phys. C **36**, 1055 (2012).